Research Article

Solid-State Synthesis of Green Mussels (*Perna viridis*)-Derived Hydroxyapatite and Perovskite Nanocomposite for the Photo-catalytic Degradation of Acetaminophen

Keren Keziah Flores Tangarorang, Fitzpatrick Devera Schmitt, Jexhee Darrel Clemente Sy, Marie Danielle Leopardas Ahongon, Piolo Miguel Vergara Garcia and Jarlie Rosario Clemeña
Department of Chemical Engineering, College of Engineering, Pamantasan ng Lungsod ng Maynila, General Luna, corner Muralla St, Intramuros, Manila, Philippines

Rugi Vicente Del Castillo Rubi* and Carlou Siga-an Eguico
Department of Chemical Engineering, College of Engineering, Adamson University, Manila, Philippines

Allan Nana Soriano, Joseph Rempillo Ortenero and Vergel Castaneda Bungay
Department of Chemical Engineering, Gokongwei College of Engineering, De La Salle University, Manila, Philippines

* Corresponding author. E-mail: rugi.vicente.rubi@adamson.edu.ph DOI: 10.14416/j.asep.2025.09.005
Received: 7 May 2025; Revised: 29 May 2025; Accepted: 29 July 2025; Published online: 15 September 2025

Abstract
Acetaminophen (ACT) emerged as the second most prevalent pharmaceutical contaminant in Philippine waters and poses environmental risks due to overuse. This study investigates the efficacy of hydroxyapatite-calcium titanate (HAp-$CaTiO_3$) nanocomposite derived from waste *Perna viridis* (green mussel) shells for the photocatalytic degradation of ACT. HAp and $CaTiO_3$ were prepared via coprecipitation and solid-state methods, respectively, and combined into a nanocomposite. The photocatalysts were characterized using SEM-EDX, XRD, UV-Vis and FTIR. Characterization confirmed the formation of a heterojunction with nanostructures and functional groups retained. The nanocomposite achieved a 96.30% ACT degradation efficiency. This approach highlights the potential of waste-derived materials for sustainable environmental remediation.

Keywords: Acetaminophen, Calcium titanate, Hydroxyapatite, Nanocomposite, Photocatalytic degradation

1 Introduction

Pharmaceutical residues are considered as emerging contaminants signifying molecules found in low concentrations (ppm or ppb) with negative effects on the environment [1]. Acetaminophen (ACT), widely known as paracetamol, is a significant emerging contaminant due to its global overuse and widespread availability [2]. Approximately 58–68% of ACT is excreted into the environment due to incomplete human metabolism [2]. Globally, ACT traces are present across all continents, with the highest concentration recorded at 227 ppb among active pharmaceutical ingredients [3]. In the Philippines, ACT is the second most prevalent pharmaceutical contaminant in natural waters, with concentrations reaching 289.17 ppb and 253.39 ppb [4]. Chronic exposure to ACT in aquatic organisms can result in reproductive system alterations, teratogenic effects, and disruptions to physiological processes [5]–[7]. This type of contaminant can have adverse ecological effects like bioaccumulation within the food chain [4]. Thus, it is crucial to develop wastewater treatment technology to effectively address these issues.

Traditional methods like activated carbon adsorption from banana peel achieve over 94.7% efficiency for initial ACT concentrations of 0.97 g/L [8]. However, these physical mechanisms only facilitate a temporary transfer of pollutants and do not entirely break them down. Biological treatments using

microorganisms or plants are environmentally friendly but slow due to high acclimation times [2]. *Pseudomonas* spp. from a hospital bioreactor degrades 200 mg/L of ACT in ~10 h [9]. An alternative method, such as chemical mechanisms, particularly photocatalytic degradation, provides sustainable, high efficiency, and cost-efficient degradation [10].

Photocatalysis involves activating a semiconductor via light exposure to produce charge carriers that degrade pollutants into simpler compounds [11]. Modified hydroxyapatite (HAp) photocatalysts have gained attention for their biocompatibility, bioactivity, nontoxicity, and cost-effectiveness [12]. Their photocatalytic properties improve when coupled with oxides like calcium titanate ($CaTiO_3$), a stable, nontoxic, and economical n-type perovskite semiconductor [13], [14]. Hence, the integration of $CaTiO_3$ to HAp could provide an opportunity to improve its overall photocatalytic performance. Recent studies have often used copper-based photocatalysts against ACT, like Cu-hsCN (94.80% degradation) [15] and $Cu_2O/WO_3/TiO_2$ (92.47% degradation) [16]. As such, in this study, a low-cost single-sourced photocatalyst is observed to degrade a prevalent contaminant, acetaminophen, from Philippine waters. Moreover, the solid-state synthesis is utilized as a novel production of the HAp-$CaTiO_3$ nanocomposite due to its facile and green process.

This study aims to explore a sustainable source of nanocomposite with hydroxyapatite and calcium titanate derived from green mussels (*Perna viridis*), also known colloquially as *tahong*. Moreover, its performance under varying operating parameters, namely catalyst loading and exposure time, was evaluated.

2 Materials and Methods

2.1 *Materials*

The main raw materials for the synthesis of HAp-$CaTiO_3$ nanocomposite were green mussel shells (*Perna viridis*), diammonium phosphate ($[NH_4]_2HPO_4$), and titanium (IV) oxide (TiO_2) anatase form. The former was acquired from a seafood market in Cavite, Philippines, and the latter two reagents from FUJIFILM Wako Pure Chemical Corporation, Japan. Additionally, Acetaminophen, a pharmaceutical secondary standard and certified reference material, was acquired from Sigma-Aldrich, Germany.

2.2 *HAp-$CaTiO_3$ synthesis*

The pre-treatment of raw material, *tahong*, involved boiling, rinsing, and grinding prior to calcination. The ground *tahong* was subjected to calcination using a Nabetherm muffled furnace at 1000 ℃ for 2 h to obtain calcium oxide (CaO) powder. The acquired CaO serves as the calcium source for both the HAp and $CaTiO_3$.

Subsequently, hydroxyapatite synthesis via co-precipitation was carried out following the methodology detailed in related literature [17]. A solution of 400 g/L calcium oxide in 250 mL was initially prepared. A 566g/L aqueous diammonium phosphate ($[NH_4]_2HPO_4$) solution in 250 mL was intermittently added at a gradual rate of 5 mL per minute to the calcium oxide solution. It was agitated using a magnetic stirrer for 60 min at a temperature of 70 ℃. After exhausting the diammonium phosphate, the pH of the mixture was regulated to be above 9 by introducing 3M ammonium hydroxide (NH_4OH, 25%). The mixture was continually stirred for an additional 50 min at 70 ℃. The resulting solution was then subjected to an aging process for 24 h and rinsed with distilled water. The solution was filtered to obtain the precipitate of HAp. The precipitate was dried in a Shel Lab 1600 Hafo Series convection drying oven at 100 ℃ for 2 hours to obtain pure HAp. Finally, the oven-dried HAp was calcined at 950 ℃ for 3 h.

Furthermore, the synthesis methodology for $CaTiO_3$ was derived from an adapted approach [18]. The CaO powder obtained from calcination was combined with Titanium Dioxide at a Ca:Ti molar ratio of 1:1 and subjected to grinding using Ogawa Seiki Co. Laboratory Mill 16986 prior to calcination at 400 °C for a duration of 4 h.

Lastly, the synthesis of HAp-$CaTiO_3$ nanocomposite was adopted from the proposed methodology by Sri-o-Sot *et al*. [19]. A 2:3 mass ratio of perovskite and hydroxyapatite undergoes 16 h of grinding in an automatic mortar and pestle in a wet environment, utilizing acetone as the solvent. The objective is to achieve the homogenization of these distinct powders. Subsequently, the resulting nanocomposite undergoes a drying process in an oven set at a temperature of 120 °C for a duration of 6 h.

2.3 *Catalyst characterization*

The $CaTiO_3$, HAp, and HAp-$CaTiO_3$ sample powder were characterized to analyze their size, shape, composition, and surface properties at the nanoscale, enabling the researchers to comprehend and control their unique properties for the photocatalytic degradation of acetaminophen. The microscopic surface features and particle dimensions of the synthesized nanocomposites were analyzed using Scanning Electron Microscopy with Energy-Dispersive X-ray Spectroscopy (SEM-EDX). The crystalline arrangements and structures of these nanocomposites were evaluated using X-ray Diffraction (XRD). UV-Vis Spectroscopy was used to determine the excitation wavelength and the band gap using a Tauc plot of the catalyst using a Shimadzu UV-1900i UV-vis spectrophotometer. Lastly, Fourier Transform Infrared Spectroscopy (FTIR) was employed to identify the chemical composition and functional groups within the photocatalysts.

2.4 *Photocatalytic degradation of acetaminophen*

The photocatalytic degradation of acetaminophen was adopted from similar literature [20]. It was carried out initially with the production of the acetaminophen mother solution. A 100 ppm solution with 100 mg of pure acetaminophen powder dissolved in 1 L of distilled water was prepared. It was contained in an amber bottle and stored in a freezer to prevent concentration fluctuation and chemical losses. The controlled initial pollutant concentration of 10 ppm was derived via serial dilution from the prepared mother solution.

In the photocatalytic degradation process, 100 mL of reaction volume with 10 mL of ACT solution was prepared. A varying photocatalyst load of 1.5 g/L, 2 g/L, and 2.5 g/L (mass of catalyst per reaction volume) was added. The solution's pH was maintained at 6 using 0.1 M sodium hydroxide (NaOH) and hydrochloric acid (HCl). Hydrogen peroxide (H_2O_2) was added at a concentration of 7mM for additional oxygen to produce more hydroxyl radicals. After adding the catalyst, the mixture was agitated in the dark for 1 hour to reach adsorption-desorption equilibrium.

The solution was then exposed to a 180 W ultraviolet lamp under magnetic stirring maintained at ambient temperature (24 °C). At 30-minute intervals over a 120-minute period, samples of the supernatant solution were withdrawn and filtered. The remaining concentration of acetaminophen was determined through a Shimadzu UV-1900i UV-vis spectrophotometer, measuring the absorbance at the wavelength of 243 nm.

3 Results and Discussion

3.1 *Characterization of HAp, $CaTiO_3$, and HAp-$CaTiO_3$*

The hydroxyapatite (HAp), calcium titanate ($CaTiO_3$), and hydroxyapatite-calcium titanate (HAp-$CaTiO_3$) nanocomposite were characterized using Scanning Electron Microscopy with Energy-Dispersive X-ray Spectroscopy (SEM-EDX), Fourier Transform Infrared (FTIR) spectroscopy, X-Ray Diffraction (XRD) analysis, and UV-Vis analysis.

3.1.1 X-ray Diffraction (XRD)

The diffraction peaks of the HAp-$CaTiO_3$ nanocomposite were indexed to hexagonal and orthorhombic structures, confirming HAp and $CaTiO_3$ phases through the RRuff database (IDs R050512 and R060345, respectively). The HAp has the following lattice parameters: a=9.39Å, b=9.39Å and c=6.86Å. On the other hand, the $CaTiO_3$ has the following lattice parameters: a=5.29Å, b=5.54Å and c=8.19Å. The sharp, intense diffraction top peaks at 25.47°, 31.97°, and 33.1°, as shown in Figure 1, confirm the crystalline nature of the HAp-$CaTiO_3$ nanocomposite. In addition, a higher intensity for HAp peaks suggests a higher content of the hydroxyapatite phase compared to $CaTiO_3$. The (211) orientation showed the highest intensity, aligning with the existing study [17]. Low-intensity peaks were attributed to background noise. The average crystallite sizes of HAp and $CaTiO_3$ are 76.05 nm and 63.54 nm, respectively. The HAp-$CaTiO_3$ nanocomposite has an average crystallite size of 90.17 nm.

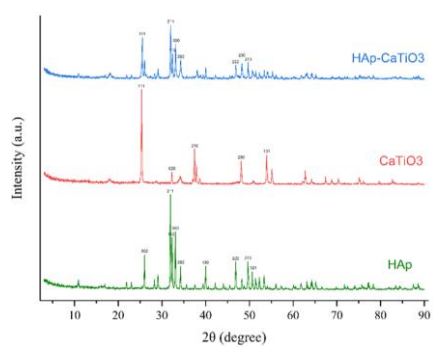

Figure 1: XRD results of the HAp, $CaTiO_3$, and HAp-$CaTiO_3$ nanocomposite.

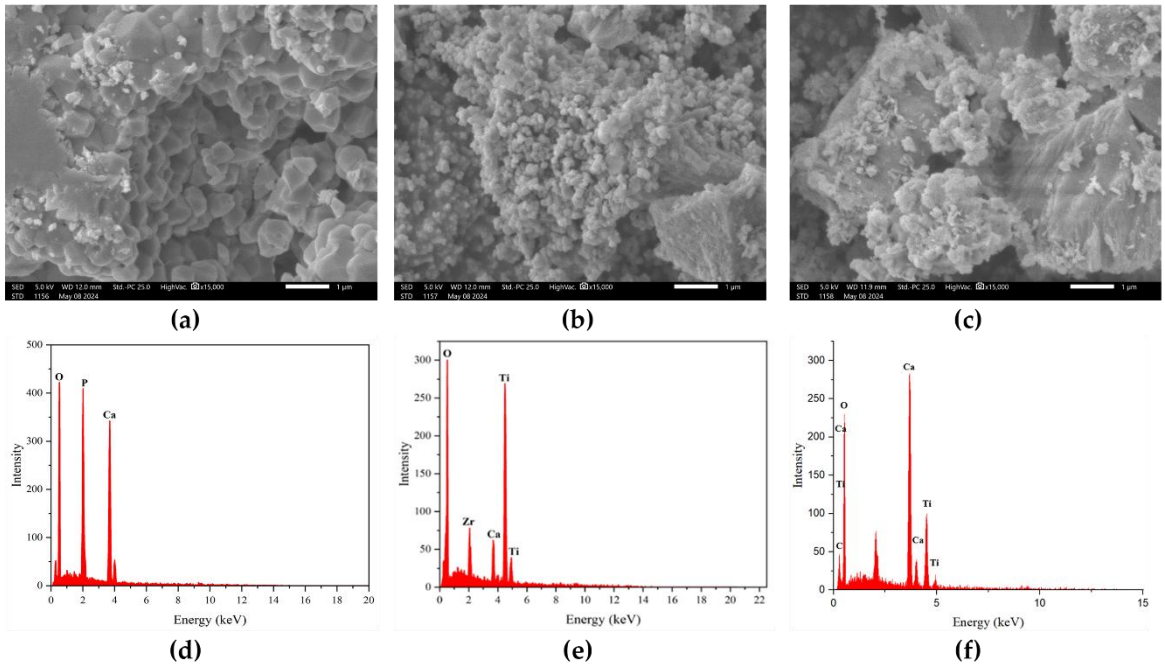

Figure 2: SEM results of photocatalysts: (a) HAp, (b) CaTiOn, and (c) HAp-CaTiOn. EDX results of photocatalysts: (d) HAp, (e) $CaTiO_3$, and (f) HAp-$CaTiO_3$.

3.1.2 Scanning electron microscopy with energy-dispersive X-ray spectroscopy (*SEM-EDX)*

Figure 2 shows the SEM-EDX images of HAp, $CaTiO_3$ and HAp-$CaTiO_3$. It showed that HAp particles have an irregular polyhedral shape with an average size of 533 nm. Individual grains are distinguishable, suggesting crystallinity, which is consistent with findings in [21].

Subjecting to higher temperature, the crystal structure of the composite grows sharper and high peaks representing a high crystallinity on the XRD result [22]. While calcium titanate has nanoclusters with an average distribution of 81.78 nm, aligning with characteristics reported [18]. There is evidence of interstitial spaces between uneven particles, which provide active sites for interaction with pollutants.

For HAp-$CaTiO_3$ micrograph showed a mix of large polyhedral structures and smaller, granular particles with 73 nm average size attached to these plates. The presence of smaller clusters aligns with the study, which also employed a solid-state method [22].

The irregularity of shape was a consequence of solid-state synthesis. When reactions are purely in the solid phase, phase heterogeneity could happen if there's uneven diffusion or localized reaction [11]. The combination of these features results in a rough and layered structure, which is commonly preferred in photocatalysis.

EDX analysis from Figure 2 confirmed the presence of elemental O, P, and Ca in HAp, consistent with [17], [23]. For $CaTiO_3$, Ca, Ti, and O were detected, aligning with similar studies [25]. In the nanocomposite, EDX detected Ca, Ti, and O, but P was absent, possibly due to the point-specific nature of the technique and structural heterogeneity. The findings affirm the composition and heterojunction formation, as supported by prior studies [17]–[25].

3.1.3 UV-Vis Spectroscopy

Figure 3 shows UV-Vis absorption spectra of $CaTiO_3$ (perovskite), hydroxyapatite (HAp), and the HAp–$CaTiO_3$ nanocomposite, which were analyzed to investigate their optical and electronic properties.

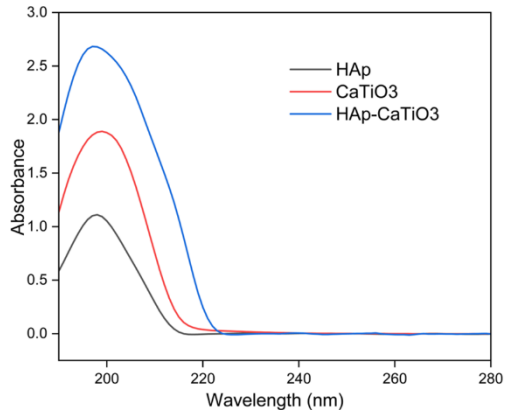

Figure 3: UV-Vis result of hydroxyapatite (HAp), perovskite ($CaTiO_3$), Hap-$CaTiO_3$ nanocomposite.

As shown in Figure 3, the absorption edges of the individual materials and the nanocomposite exhibit characteristic peaks around 200 nm, with notable absorbance features at approximately 1.1 eV, 1.9 eV, and 2.7 eV. These peaks are attributed to π–π* electronic transitions and charge transfer processes, which are indicative of the ion exchange mechanisms occurring within the crystal lattices of both perovskite and hydroxyapatite structures [26]. The absorption behavior of the nanocomposite closely resembles that of the individual components, suggesting that the intrinsic optical properties of HAp and $CaTiO_3$ are preserved within the composite structure. However, a significant increase in overall absorbance is observed for the HAp–$CaTiO_3$ nanocomposite compared to its individual constituents. This enhancement indicates synergistic interaction between the HAp and $CaTiO_3$ phases, likely resulting in improved electronic coupling and a more effective cation-exchangeable framework. The interfacial charge transfer between the components contributes to increased photoactivity and light-harvesting capability, which can enhance the composite's performance in applications, such as photocatalysis or adsorption-driven processes [27].

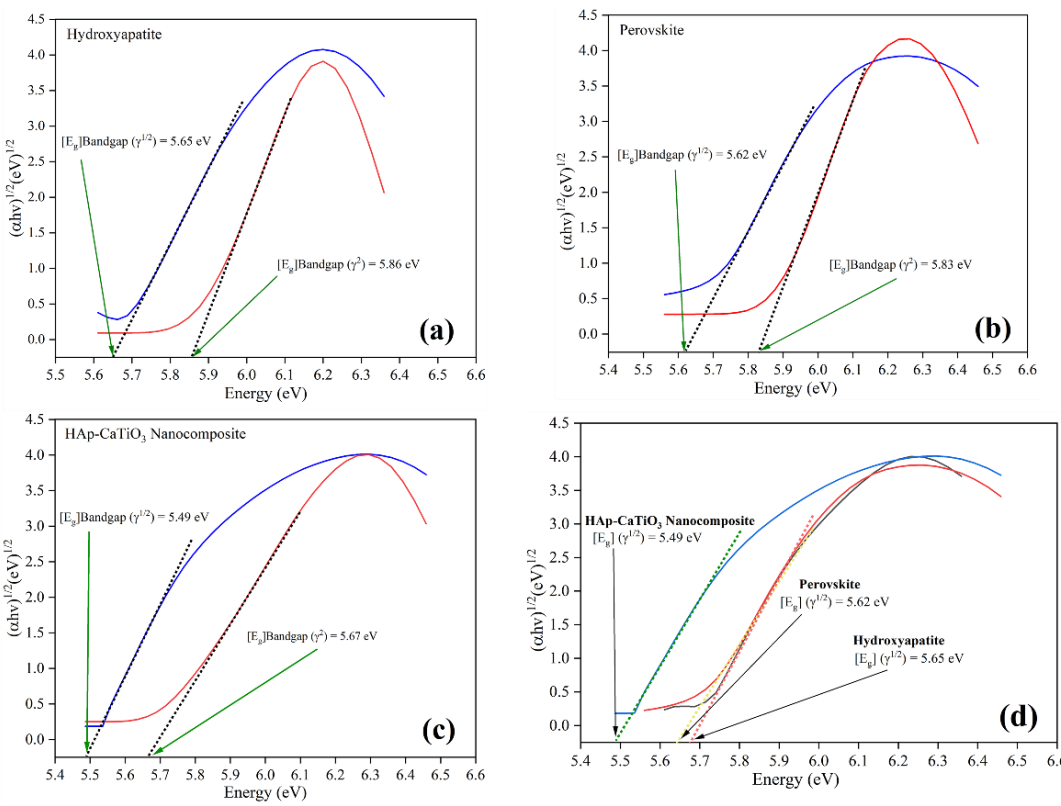

Figure 4: Tauc plot results of the (a) HAp, (b) perovskite or $CaTiO_3$, (c) HAp-$CaTiO_3$ nanocomposite, and comparison of (a), (b), and (c).

Interestingly, the nanocomposite exhibited a band gap range of 5.49–5.65 eV as indicated in Figure 4, which is significantly larger than that of typical adsorbent materials, such as activated carbon or other transition metal oxides [28]. However, when comparing the individual components to the composite (Figure 4(d)), it is evident that the band gap of the nanocomposite is slightly narrower than that of the pristine HAp and $CaTiO_3$. This narrowing is attributed to the synergistic interaction between HAp and $CaTiO_3$, leading to improved electron delocalization at the interface, which can facilitate electron mobility and enhance surface reactivity [29]. A larger band gap often contributes to better thermal and chemical stability, which is desirable for adsorbents operating under harsh environmental conditions. Moreover, in specific adsorption processes where photogenerated charge carriers play a role (e.g., photocatalytic adsorption or UV-assisted adsorption), an optimized band gap can enhance the material's performance by reducing unwanted recombination rates [30].

3.1.4 Fourier transform infrared spectroscopy (FTIR)

The results of the FTIR reading displayed in Figure 5 show peaks at 3636, 1546, 1085, 820, and 599 cm^{-1}. At 3636 cm^{-1}, observed above 3000 cm^{-1}, suggests the presence of OH- stretching, which may be due to the moisture adsorbed during the synthesis or testing [31]. No peaks were detected between 2500 cm^{-1} to 2000 cm^{-1}, which suggests that no carbon triple bonds are present for all samples. At wavenumber between 2000 cm^{-1} and 1500 cm^{-1}, one peak was observed at around 1546 $cm^{-1,}$ which suggests double bond stretches in $CaTiO_3$, HAp, and HAp-$CaTiO_3$.

For the wavenumber below 1500 cm^{-1}, three peaks were observed. The 1085 cm^{-1} is present on both HAp and HAp-$CaTiO_3$, which signifies the bending modes of stretching (P-O) mode of PO_4^{3-} [17]. The 820 cm^{-1} is a specific vibration of the bond of Ca-Ti-O, which is expectedly present on both $CaTiO_3$ and HAp-$CaTiO_3$ but absent in HAp [31]. Lastly, 599 cm^{-1} is the vibration of the phosphate group found in HAp and HAp-$CaTiO_3$ [17].

Notably, significant differences in peak intensity at 1546 cm^{-1} between individual catalysts and the nanocomposite may result from the solid-state synthesis method employed, which affected the molecular interactions of the pristine semiconductors, causing a slight change in peak intensity. Nevertheless, the shift in characteristic peak at around 1546 cm^{-1} of the nanocomposite compared to the individual catalysts indicates strong molecular interaction and formation of new bonds. Additionally, the three major peaks in the fingerprint region at 820 cm^{-1} in $CaTiO_3$, and 1085 cm^{-1} and 599 cm^{-1} in HAp, were retained, showing shifts of intensity in the nanocomposite that correspond to the bonding interaction of HAp and $CaTiO_3$, thus confirming the successful heterojunction formation between the two individual semiconductors [32].

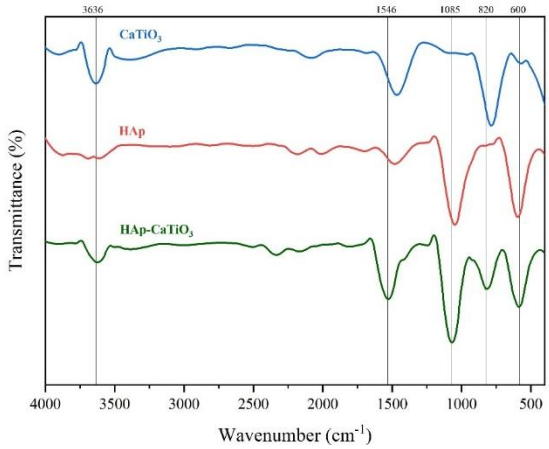

Figure 5: FTIR results of the HAp, $CaTiO_3$, and HAp-$CaTiO_3$ nanocomposite.

3.2 *Photocatalytic degradation of Acetaminophen*

The highest photocatalytic efficiency was observed at a catalyst loading of 2.0 g/L. The efficiency increases from 1.5 g/L (89.69%) to 2.0 g/L (96.30%) but slightly decreases at 2.5 g/L (94.49%), as highlighted in Figure 6. This indicates that beyond a catalyst concentration of 2 g/L, increasing the catalyst loading does not continue to improve performance and may even reduce it. The decrease in efficiency at 2.5 g/L might be due to saturation effects, where excess catalyst does not contribute to increased photocatalytic activity and could lead to issues like light scattering or reduced active surface area exposure [18]. Similar studies that degrade acetaminophen showed 94.80% with SACu-hsCN and ZnO-NiO Nanofibers catalyst showed 92% degradation efficiency in 3 h [15], [33]. This study has achieved an effective degradation efficiency with a sustainable source, *tahong*.

The photocatalytic degradation relies on the number of photons that reach the catalyst and activate the generation of electron-hole pairs. The free

photoelectron in the conduction band facilitates the creation of reactive oxygen species (such as hydroxyl radical OH•) within the composite [34]. The radicals create a chain reaction that could partially degrade the ACT to by-products and then completely mineralize it to CO_2 and H_2O [35].

To get a better understanding of the mechanism of the nanocomposite decomposition of ACT, individual catalysts were observed under identical conditions. The percent degradation of acetaminophen using various types of catalysts is shown in Figure 7. Notably, the no-catalyst control group exhibited minimal degradation of 3.56%, highlighting the resilience of ACT on typical wastewater.

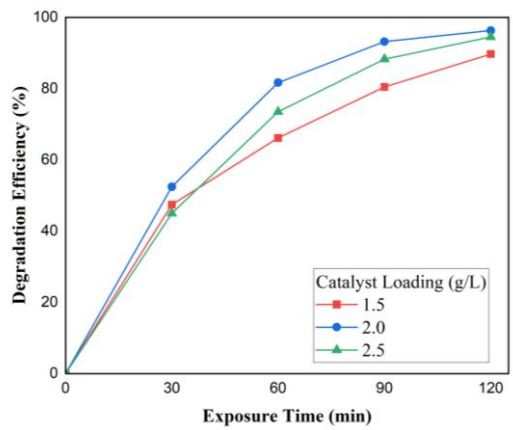

Figure 6: Percent degradation vs. time of (a) HAp-$CaTiO_3$ catalysts at varying catalyst load (1.5 g/L, 2.0 g/L, 2.5 g/L).

HAp showed 89.5 % degradation for ACT in 120 mins, as shown in Figure 6, compared to similar studies that resulted in minimal ACT degradation [36]. The results can be attributed to the added calcination step to the HAp synthesis. The calcination step provided oxygen vacancies on the HAp and lowered its band gap energy [37]. The lower band gap enhances light absorption and photocatalytic activity, leading to the observed increase in ACT degradation. While calcium titanate, a novel photocatalyst, demonstrated 64.53% degradation efficiency against acetaminophen. Mostafa *et al*. reported a 3.0–3.5 eV bandgap for calcium titanate derived from *Perna viridis*, classifying it as UV-active [38]. This bandgap enables light absorption for wavelengths under 387 nm, primarily within the ultraviolet range [39].

Thus, HAp, with its naturally porous structure and induced oxygen vacancies, facilitates the adsorption of pollutants and improves contact with the photocatalyst. While $CaTiO_3$ contributes additional active sites for photocatalytic reactions. When combined, the overall availability of active sites increases, allowing for more effective degradation of pollutants like acetaminophen.

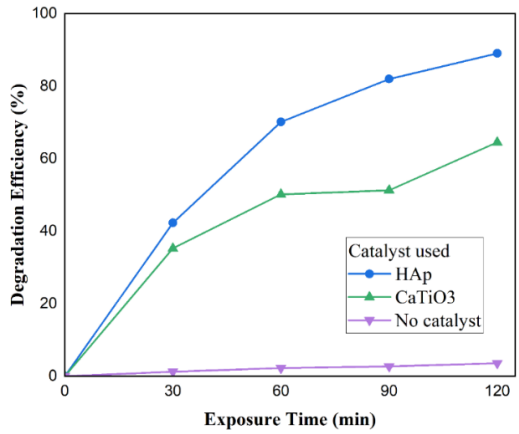

Figure 7: Percent degradation vs. time of HAp, $CaTiO_3$ and no catalyst.

3.3 *Statistical Treatment*

Two-way analysis of variance (ANOVA) was conducted to assess the effects of catalyst loading and exposure time on acetaminophen degradation. Results showed that both catalyst loading (p-value < 0.0001) and exposure time (p-value < 0.0001) significantly influenced degradation efficiency. However, their interaction (p-value = 0.09587) was not statistically significant, indicating independent effects on the response variable.

Figure 8 presents the contour plot of acetaminophen degradation at varying exposure times and catalyst loadings (10 ppm initial concentration). Closely packed lines in the lower section indicate rapid degradation from 0 to 60 min, while wider gaps beyond 60 minutes suggest diminishing effects. Steeper lines between 30- and 60-min highlight catalyst loading's increasing impact, with 2 g/L showing the most intense response. Maximum degradation occurs at 120 min and around 2 g/L catalyst loading.

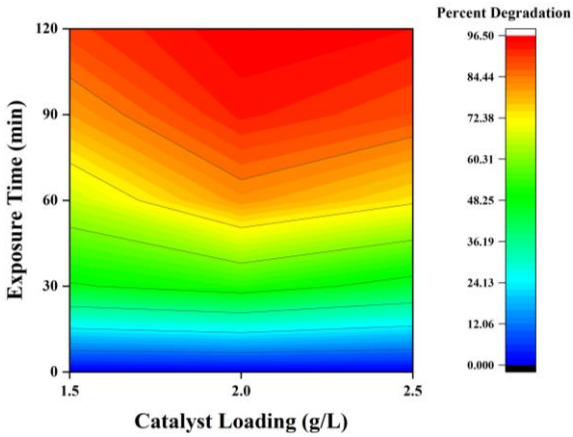

Figure 8: Contour plot of percent degradation vs. exposure time vs. catalyst loading at 10 ppm initial pollutant concentration.

For Figure 9, the response surface plot further supports these findings, showing an overall upward trend in degradation with time. Efficiency peaks at a catalyst loading of 2 g/L, beyond which efficiency declines, indicating system saturation. The color gradient intensifies at higher exposure times, with 2 g/L achieving a quicker response. This suggests that prolonged exposure enhances degradation, while 2 g/L represents the optimal catalyst concentration.

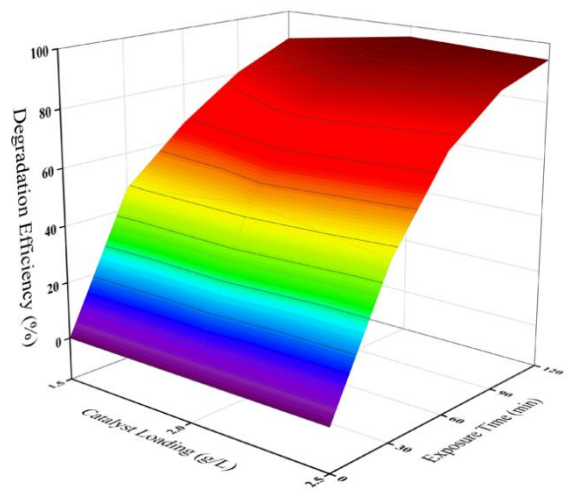

Figure 9: Response surface plot of percent degradation vs. exposure time vs. catalyst loading at 10 ppm initial pollutant concentration.

4 Conclusions

Waste *Perna viridis* (green mussel) shells were utilized on the synthesis of HAp and $CaTiO_3$ photocatalyst. Successful formation of HAp-$CaTiO_3$ nanocomposite via solid-state was confirmed by collective analysis of XRD, FTIR, UV-Vis and SEM-EDX techniques. The polyhedral structure of HAp and clustered structure of $CaTiO_3$ were observed resulting in a flowery structure of the nanocomposite, particle crystallite size was found in the nano region, and shift in peak intensity signatures of individual catalysts were found on the nanocomposite, suggesting molecular interaction and formation of new bonds. The synthesized HAp-$CaTiO_3$ exhibited the highest photocatalytic efficiency (96.53%) at the catalyst loading of 2.0 g/L and exposure time of 120 minutes, compared to the individual HAp (89.5%) and $CaTiO_3$ (64.53%) catalysts. This study presents a novel approach for utilizing waste *Perna viridis* shells as a precursor for a single-sourced photocatalyst. The successful synthesis and characterization of the HAp, $CaTiO_3$, and HAp-$CaTiO_3$ nanocomposite demonstrate their potential as a sustainable and efficient material for ACT degradation. While the study highlights the photocatalytic potential of the HAp-$CaTiO_3$ nanocomposite, its reusability under repeated photocatalytic cycles remains unexplored. Further research is recommended to evaluate the catalyst's efficiency and stability over multiple uses to better assess its practical application in real wastewater treatment systems.

Acknowledgments

The researchers express their sincere gratitude to the Pamantasan ng Lungsod ng Maynila (PLM) Chemical Engineering Department and Science Laboratory Services (SLS) for their unwavering support in the completion of this research. They also extend their appreciation to De La Salle University Chemical Engineering Department for their assistance in acquiring the necessary materials and financial aid essential to research methodology. Special thanks to Adamson University for Biomass, Energy and Nanotechnology (ALBEN) for their valuable guidance and insights into the development of this research. The contributions of these institutions have been truly irreplaceable, and the generosity shown to the researchers is deeply appreciated.

Author Contributions

D.L.A.: conceptualization, investigation, methodology, data curation; P.M.V.G.: conceptualization, investigation, methodology, data curation; F.D.S.: conceptualization, investigation, methodology, data curation, data analysis, methodology, writing—reviewing and editing; J.D.C.S.: conceptualization, investigation, methodology, data curation, data analysis, methodology, writing—reviewing and editing; K.K.F.T.: conceptualization, investigation, methodology, data curation, data analysis, methodology, writing—reviewing and editing; A.N.S.: conceptualization, characterization, writing—reviewing and editing; J.R.O.: conceptualization, characterization, writing—reviewing and editing; V.C.B.: writing—reviewing and editing; R.V.C.R., R.S.E: conceptualization, characterization, supervision, writing—reviewing and editing; J.R.C: supervision. All authors have read and agreed to the published version of the manuscript.

Conflicts of Interest

The authors declare no conflict of interest.

References

[1] C. A. Aguilar et al., "Effect of kinetics on the photocatalytic degradation of acetaminophen and the distribution of major intermediate with anatase-Ag synthesized by sol gel under visible irradiation," *Frontiers in Environmental Science*, vol. 10, Oct. 2022, doi: 10.3389/fenvs.2022.943776.

[2] Z. Wang et al., "Photocatalytic degradation of acetaminophen in aqueous environments: A mini review," *Toxics*, vol. 11, no. 7, pp. 604, Jul. 2023, doi: 10.3390/toxics11070604.

[3] J. L. Wilkinson et al., "Pharmaceutical pollution of the World's Rivers," in *Proceedings of the National Academy of Sciences*, Feb. 2022, vol. 119, no. 8, doi: 10.1073/pnas.2113947119.

[4] S. M. F. Mariano, L. F. Angeles, D. S. Aga, C. L. Villanoy, and C. M. B. Jaraula, "Emerging pharmaceutical contaminants in key aquatic environments of the Philippines," *Frontiers in Earth Science*, vol. 11, Sep. 2023, doi: 10.3389/feart.2023.1124313.

[5] W. Koagouw, N. A. Stewart, and C. Ciocan, "Long-term exposure of marine mussels to paracetamol: Is time a healer or a killer?" *Environmental Science and Pollution Research*, vol. 28, no. 35, pp. 48823–48836, Apr. 2021, doi: 10.1007/s11356-021-14136-6.

[6] V. P. Cedron, A. M. J. Weiner, M. Vera, and L. Sanchez, "Acetaminophen affects the survivor, pigmentation and development of craniofacial structures in zebrafish (Danio rerio) embryos," *Biochemical Pharmacology*, vol. 174, p. 113816, Apr. 2020, doi: 10.1016/j.bcp.2020.113816.

[7] E. Choi, D. Alsop, and J. Y. Wilson, "The effects of chronic acetaminophen exposure on the kidney, gill and liver in rainbow trout (Oncorhynchus mykiss)," *Aquatic Toxicology*, vol. 198, pp. 20–29, May 2018, doi: 10.1016/j.aquatox.2018.02.007.

[8] T. Mukherjee and M. Rahaman, "Optimization of acetaminophen adsorption onto biodegradable waste-derived activated carbon using response surface methodology," *Materials Today Proceedings*, vol. 76, pp. 233–238, Jan. 2023, doi: 10.1016/j.matpr.2023.01.051.

[9] A. B. Rios-Miguel, G. J. Smith, G. Cremers, T. van Alen, M. S. M. Jetten, H. J. M. Op Den Camp, and C. U. Welte, "Microbial Paracetamol Degradation Involves a High Diversity of Novel Amidase Enzyme Candidates," *Water Research X*, vol. 16, p. 100152, Aug. 2022, doi: 10.1016/j.wroa.2022.100152.

[10] A. Saravanan, P. S. Kumar, S. Jeevanantham, M. Anubha, and S. Jayashree, "Degradation of toxic agrochemicals and pharmaceutical pollutants: Effective and alternative approaches toward photocatalysis," *Environmental Pollution*, vol. 298, p. 118844, Apr. 2022, doi: 10.1016/j.envpol.2022.118844.

[11] R. L. P. Rocha, L. M. C. Honorio, R. D. D. S. Bezerra, P. Trigueiro, T. M. Duarte, M. G. Fonseca, E. C. Silva-Filho, and J. A. Osajima, "Light-activated hydroxyapatite photocatalysts: New environmentally-friendly materials to mitigate pollutants," *Minerals*, vol. 12, no. 5, p. 525, Apr. 2022, doi: 10.3390/min12050525.

[12] S. Panda, C. K. Biswas, and S. Paul, "A comprehensive review on the preparation and application of calcium hydroxyapatite: A special focus on atomic doping methods for bone tissue engineering," *Ceramics International*, vol. 47, no. 20, pp. 28122–28144, Oct. 2021, doi: 10.1016/j.ceramint.2021.07.100.

[13] E. Márquez Brazón, C. Piccirillo, I. S. Moreira, and P. M. L. Castro, "Photodegradation of pharmaceutical persistent pollutants using hydroxyapatite-based materials," *Journal of*

Environmental Management, vol. 182, pp. 486–495, Nov. 2016, doi: 10.1016/j.jenvman.2016.08.005.

[14] M. Passi and B. Pal, "A review on $CaTiO_3$ photocatalyst: Activity enhancement methods and photocatalytic applications," *Powder Technology*, vol. 388, pp. 274–304, Aug. 2021, doi: 10.1016/j.powtec.2021.04.056.

[15] S. Tian, Y. Yin, M. Liu, L. Shi, S. Zhang, A. H. Asif, X. Li, M. Liu, X. Duan, S. Wang, and H. Sun, "Atomically dispersed Cu-N_3 on hollow spherical carbon nitride for acetaminophen degradation: Generation of O_2 from H_2O_2," *Separation and Purification Technology*, vol. 318, p. 124016, May 2023, doi: 10.1016/j.seppur.2023.124016.

[16] J. H. F. Chau, C. W. Lai, B. F. Leo, J. C. Juan, and M. R. Johan, "Advanced photocatalytic degradation of acetaminophen using $Cu_2O/WO_3/TiO_2$ ternary composite under solar irradiation," *Catalysis Communications*, vol. 163, p. 106396, Mar. 2022, doi: 10.1016/j.catcom.2022.106396.

[17] M. Sari and Y. Yusuf, "Synthesis and characterization of hydroxyapatite based on green mussel shells (perna viridis) with the variation of stirring time using the precipitation method," *IOP Conference Series: Materials Science and Engineering*, vol. 432, p. 012046, Nov. 2018, doi: 10.1088/1757-899x/432/1/012046.

[18] I. Fatimah, R. N. Ilahi, and R. Pratami, "Low cost $CaTiO_3$ Perovskite synthesized from Scallop (*Anadara granosa*) shell as antibacterial ceramic material," *IOP Conference Series: Materials Science and Engineering*, vol. 299, p. 012034, Jan. 2018, doi: 10.1088/1757-899x/299/1/012034.

[19] S. Sri-o-Sot, K. Vepulanont, T. Pitakpornpreecha, A. Aroonkesorn, A. Charoenpanich, T. Srichumpong, and T. Chanadee, "$CaTiO_3$-hydroxyapatite bioceramic composite: Synthesis of reactant powders from waste cockle shell, sintering, characterization and investigation of physical, mechanical and in-vitro biological properties," *Journal of the Australian Ceramic Society*, vol. 60, pp. 65–87, Dec. 2023, doi: 10.1007/s41779-023-00987-4.

[20] M. T. D. C. Español, E. R. J. G. Garcia, L. A. V. Maligaya, C. M. S. Santos, J. A. Santos, N. G. Suarnaba, R. V. C. Rubi, and R. Raguindin, "Ultrasound-assisted biomimetic synthesis of MOF-Hap nanocomposite via 10xSBFLike for the photocatalytic degradation of metformin," *Applied Science and Engineering Progress*, vol. 17, no. 2, p. 7251, Apr. 2024, doi: 10.14416/j.asep.2023.11.002.

[21] S. C. Wu, H. C. Hsu, W. H. Wu, and W. F. Ho, "Enhancing bioactivity and mechanical properties of nano-hydroxyapatite derived from oyster shells through hydrothermal synthesis," *Nanomaterials*, vol. 14, no. 15, p. 1281, Jul. 2024, doi: 10.3390/nano14151281.

[22] C. S. Eguico, M. M. Abanto, H. T. Cendaña, D. A. P. Famero, K. B. Pediongco, A. D. C. Evangelista, R. V. C. Rubi, "Sonophotopythochemical functionalization of graphene Oxide-Al-Zn bimetal nanocomposite for corrosion inhibition," *Applied Science and Engineering Progress*, vol. 18, no. 2, p. 7613, Oct. 2024, doi: 10.14416/j.asep.2024.10.004.

[23] K. Ponhan, K. Tassenberg, D. Weston, K. G. M. Nicholls, and R. Thornton, "Effect of SiC nanoparticle content and milling time on the microstructural characteristics and properties of Mg-SiC nanocomposites synthesized with powder metallurgy incorporating high-energy ball milling," *Ceramics International*, vol. 46, no. 17, pp. 26956–26969, Dec. 2020, doi: 10.1016/j.ceramint.2020.07.173.

[24] B. Maleki, M. Chahkandi, R. Tayebee, S. Kahrobaei, H. Alinezhad, and S. Hemmati, "Synthesis and characterization of nanocrystalline hydroxyapatite and its catalytic behavior towards synthesis of 3,4-disubstituted isoxazole-5(4H)-ones in water," *Applied Organometallic Chemistry*, vol. 33, no. 10, Jul. 2019, doi: 10.1002/aoc.5118.

[25] N. Vijayakumar, S. K. Venkatraman, S. Imthiaz, E. A. Drweesh, M. M. Elnagar, S. Koppala, S. Swamiappan, "Synthesis and characterization of calcium and magnesium-based oxides and titanates for photocatalytic degradation of rhodamine B: a comparative study," *Scientific Reports*, vol. 13, Art. no. 3615, Mar. 2023, doi: 10.1038/s41598-023-30013-3.

[26] A. Mocanu, O. Cadar, P. T. Frangopol, I. Petean, G. Tomoaia, G. A. Paltinean, C. P. Racz, O. Horovitz, and M. Tomoaia-Cotisel, "Ion release from hydroxyapatite and substituted hydroxyapatites in different immersion liquids: in vitro experiments and theoretical modelling study," *Royal Society Open Science*, vol. 8, no. 1, p. 201785, Jan. 2021, doi: 10.1098/rsos.201785.

[27] F. Vento, A. Nicosia, L. Mezzina, G. Raciti, A. Gulino, M. Condorelli, L. D'Urso, G. De Guidi, and P. Mineo, "Photocatalytic activity of TiO_2-containing nanocomposites versus the chemical nature of the polymeric matrices: A comparison," *Advanced Materials Technologies*, vol. 8, no. 17, May 2023, doi: 10.1002/admt.202300391.

[28] R. Sazonov, G. Kholodnaya, D. Ponomarev, O. Lapteva, F. Konusov, R. Gadirov, and I. Zhirkov, "Pulsed plasma chemical synthesis of TiO_2@$Ti_xC_yO_z$ nanocomposite," *Fullerenes Nanotubes and Carbon Nanostructures*, vol. 29, no. 8, pp. 567–575, Jan. 2021, doi: 10.1080/1536383x.2020.1871331.

[29] H. Xian, L. Tang, Z. Mao, J. Zhang, and X. Chen, "Synergistic effects of Ca^{2+} and high-valence Nb^{5+} co-doping on the structural, optical and magnetic properties of $BiFeO_3$," *Research Square*, Apr. 2021, doi: 10.21203/rs.3.rs-182253/v1.

[30] P. Li, F. Liu, Y. Liu, R. Xue, and X. Fan, "Preparation and photocatalytic activity of visible light-responsive zinc oxide/activated carbon fiber composites," *Journal of Dispersion Science and Technology*, vol. 42, no. 6, pp. 846–857, Jan. 2020, doi: 10.1080/01932691.2019.1711110.

[31] S. Rongsawat, W. Bunma, and T. Chanadee, "In situ combustion synthesis in air of calcium titanate powders using minerals as a calcium source," *Materials Science Forum*, vol. 982, pp. 20–25, Mar. 2020, doi: 10.4028/www.scientific.net/msf.982.20.

[32] M. I. A. Abdel Maksoud, S. Abdelhaleem, E. K. Tawfik, and A. S. Awed, "Gamma radiation-induced synthesis of novel PVA/Ag/$CaTiO_3$ nanocomposite film for flexible optoelectronics," *Scientific Reports*, vol. 13, Art. no. 12385, Jul. 2023, doi: 10.1038/s41598-023-38829-9.

[33] H. E. Gomaa, H. H. El-Maghrabi, F. A. Gomaa, P. Raynaud, and A. A. Nada, "Enhanced photodegradation of acetaminophen using efficient ZnO-NiO nanofibers," *Catalysts*, vol. 14, no. 7, p. 403, Jun. 2024, doi: 10.3390/catal14070403.

[34] H. Bouyarmane, C. El Bekkali, J. Labrag, I. Essaidi, O. Bouhnik, H. Abdelmoumen, A. Laghzizil, J-M. Nunzi, and D. Robert, "Photocatalytic degradation of emerging antibiotic pollutants in waters by TiO_2/Hydroxyapatite nanocomposite materials," *Surfaces and Interfaces*, vol. 24, p. 101155, Jun. 2021, doi: 10.1016/j.surfin.2021.101155.

[35] Y. Yuan, W-L. Wang, Z-W. Wang, J. Wang, and Q-Y. Wu, "Single-atom Ag-loaded carbon nitride photocatalysts for efficient degradation of acetaminophen: The role of Ag-atom and O_2," *Journal of Environmental Sciences*, vol. 139, pp. 12–22, May 2024, doi: 10.1016/j.jes.2023.03.042.

[36] J. Labrag, C. El Bekkali, A. Oulguidoum, D. Robert, A. Laghzizil, and J. M. Nunzi, "Porous and bifunctional ZnO-hydroxyapatite nanostructure for photocatalytic degradation of paracetamol and methylene blue in water," *Iranian Journal of Catalysis (IJC)*, vol. 11, no. 4, pp. 389–395, 2021, doi:10.57647/IJC-7ERA-ZC44.

[37] J. Zhang, C. Lv, C. Shi, J. Feng, and L. Wu, "Oxygen-vacancy hydroxyapatite for visible-light photocatalytic degradation of tetracycline with online spectral monitoring," *Microchemical Journal*, vol. 192, p. 108906, Sep. 2023, doi: 10.1016/j.microc.2023.108906.

[38] M. Mostafa, Z. A. Alrowaili, M.M. Al Shehri, M. Mobarak, and A. M. Abbas, "Structural and optical properties of calcium titanate prepared from gypsum," *Journal of Nanotechnology*, vol. 2022, no. 1 pp. 1–9, Mar. 2022, doi: 10.1155/2022/6020378.

[39] A. B. Lavand, M. N. Bhatu, and Y. S. Malghe, "Visible light photocatalytic degradation of malachite green using modified titania," *Journal of Materials Research and Technology*, vol. 8, no. 1, pp. 299–308, Jan.-Mar. 2019, doi: 10.1016/j.jmrt.2017.05.019.